ACS APPLIED MATERIALS & INTERFACES

Research Article

www.acsami.org

Thermally Induced Superhydrophilicity in TiO_2 Films Prepared by Supersonic Aerosol Deposition

Jung-Jae Park,[†] Do-Yeon Kim,[†] Sanjay S. Latthe,[†] Jong-Gun Lee,[†] Mark T. Swihart,[‡] and Sam S. Yoon*[,†]

[†]Department of Mechanical Engineering, Korea University, Seoul 136-713, Korea

[‡]Department of Chemical and Biological Engineering, The University at Buffalo, The State University of New York, Buffalo, New York 14260-4200, United States

Supporting Information

ABSTRACT: Superhydrophilic and superhydrophobic surfaces enable self-cleaning phenomena, either forming a continuous water film or forming droplets that roll off the surface, respectively. TiO_2 films are well-known for their extreme hydrophilicity and photocatalytic characteristics. Here, we describe nanostructured TiO_2 thin films prepared by supersonic aerosol deposition, including a thorough study of the effects of the annealing temperature on the crystal structure, surface morphology, surface roughness, and wetting properties. Powder X-ray diffraction showed that supersonic deposition resulted in fragmentation and amorphization of the micrometer-size anatase (60%)−rutile (40%) precursor powder and that, upon annealing, a substantial fraction of the film (~30%) crystallized in the highly hydrophilic but metastable brookite phase. The film morphology was also somewhat modified after annealing. Scanning electron microscopy and atomic force microscopy revealed rough granular films with high surface roughness. The as-deposited TiO_2 films were moderately hydrophilic with a water contact angle (θ) of ~45°, whereas TiO_2 films annealed at 500 °C became superhydrophilic ($\theta \sim 0°$) without UV illumination. This thermally induced superhydrophilicity of the TiO_2 films can be explained on the basis of the combined effects of the change in the crystal structure, surface microstructure, and surface roughness. Supersonic aerosol deposition followed by annealing is uniquely able to produce these nanostructured films containing a mixture of all three TiO_2 phases (anatase, rutile, and brookite) and exhibiting superhydrophilicity without UV illumination.

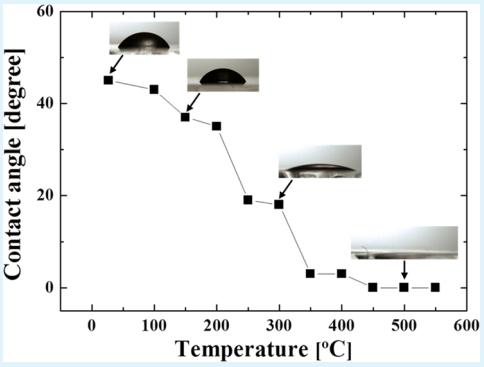

KEYWORDS: *superhydrophilic, aerosol deposition, surface roughness, wetting, annealing*

1. INTRODUCTION

Wettability is one of the key properties of a solid surface and plays important roles in daily life, agriculture, and industry. TiO_2 is the most studied and widely used photocatalyst and has been employed in many industrial applications because of its unique optical, chemical, and hydrophilic properties.[1−7] TiO_2 is inexpensive, nontoxic, inert, hard-wearing, and resistant to corrosion and chemicals and is largely impervious to photocorrosion. Significant advances have been made in the use of nanostructured titania in photocatalysis,[8] solar cells,[9,10] self-cleaning antibacterial materials, water and air purification,[11] optoelectronics,[12] cancer therapy,[13] and cathodic corrosion protection.[14] The surface properties and interactions of TiO_2, particularly with small molecules such as water, oxygen, formate, and methanol,[15−17] have been widely studied for over 30 years. The superhydrophilicity of TiO_2 thin films has attracted intense research interest because of its applications in self-cleaning and antifogging.[3] The wetting process of solids by liquids is of great technological importance. In the Wenzel regime, increased surface roughness makes hydrophobic surfaces more hydrophobic but makes hydrophilic surfaces more hydrophilic.[18] Increasing the wettability of a surface can improve its self-cleaning ability.[19] Hierarchically structured films can exhibit increased surface roughness and enhanced wettability.[20]

Recently, many hypotheses have been proposed for the hydrophilicity of TiO_2 surfaces, attributing enhanced wettability to chemical surface modification, surface topography modification, light irradiation, and thermal treatment.[7,21−28] Huang et al.[21] synthesized porous superhydrophilic TiO_2 films by a sol−gel process using poly(ethylene glycol) (PEG) as a pore-generating agent. The amount of PEG significantly affected the microstructure and hydrophilic properties of the nanoporous TiO_2 films. Hao et al.[22] investigated the size-dependent hydrophilicity of TiO_2 nanoparticles by an interface transient molecular probe method. They concluded that both the reorganization energy of the interfacial charge recombination and the density of the surface hydroxyl groups can serve as a quantitative parameter for predicting the hydrophilicity of the TiO_2 nanoparticles. Houmard et al.[23] prepared TiO_2−SiO_2 composite thin films that showed superhydrophilic behavior without UV-light irradiation. Recently, Peng et al.[24] fabricated

Received: March 26, 2013
Accepted: June 12, 2013
Published: June 12, 2013

stable superhydrophilic films ($\theta \sim 0°$) without UV irradiation. These consisted of hierarchical raspberry-like metal-ion-doped TiO_2 hollow spheres. The hierarchical surface morphology of metal-ion-doped TiO_2 hollow spheres could be programmed from "smooth" to "moderately rough" to "rough" by adjusting the molar ratio of Co^{2+} to Zn^{2+} ions. Miyauchi and Tokudome prepared transparent, adherent, and superhydrophilic titania thin films from nanotube arrays grown by the sputtering deposition of titanium films followed by hydrothermal treatment. UV illumination generated superhydrophilic states with a water contact angle of 0°. These films maintained high hydrophilicity (WCA < 5°), even after dark storage for more than 3 months, because of their surface nanostructures.[7] Du et al.[25] reported heat-induced superhydrophilicity of TiO_2 thin films doped with different amounts of Mo ions. The thermally induced hydrophilicity of nano-TiO_2 thin films deposited on silicon and quartz substrates by radio-frequency magnetron sputtering has also been reported.[26] Sebbowa et al.[27] deposited titania films on titanium alloy substrates by electrohydrodynamic atomization. These films showed a decrease in the water contact angle (from ~18° to ~9°) with increasing annealing temperature. Lai et al.[28] applied a one-step electrophoretic deposition to fabricate a transparent cross-aligned superhydrophobic titanate nanobelt fluoroalkylsilane film on a conducting glass substrate. Following thermal treatment at 500 °C, the superhydrophobic surface was converted into a superhydrophilic one.

TiO_2 films generally show high hydrophilicity under UV irradiation. However, they generally do not maintain hydrophilicity for a long period without UV irradiation. In the dark, they return to a more hydrophobic state within minutes to hours. This limits their use for numerous potential applications.[29] It is still a great challenge to fabricate superhydrophilic TiO_2 films without UV irradiation. Thermally induced hydrophilicity in TiO_2 shows promise for creating permanently hydrophilic surfaces. We report on the preparation of TiO_2 thin films by the supersonic aerosol deposition (AD) of TiO_2 particles. The effect of the annealing temperature on the crystal structure, surface morphology, surface roughness, and hydrophilicity is studied in detail. The as-deposited TiO_2 films were moderately hydrophilic, with a water contact angle of ~45°, whereas after the TiO_2 films were annealed at 500 °C, the water droplets completely spread and infiltrated the coating, demonstrating that the coating has become superhydrophilic ($\theta \sim 0°$) without UV illumination. In contrast to temporary superhydrophilicity induced by UV exposure, the superhydrophilicity of these films appears to be permanent.

2. EXPERIMENTAL SECTION

TiO_2 films were prepared on glass by supersonic AD. Figure 1 shows a schematic of the AD experimental setup, which consisted of a gas tank, a fluidized-bed powder feeder, a nozzle, a vacuum chamber, a 2D $x-y$ stage, a booster pump, and a vacuum pump. TiO_2 powder was premixed with dry air in a fluidized bed and fed to a converging–diverging nozzle. Particle-laden air was injected at supersonic velocity into a deposition chamber, which was evacuated by vacuum and booster pumps (P_{amb} = 0.35–5.6 Torr) to minimize TiO_2 particle deceleration before impact. The experimental conditions are summarized in Table 1. Schlieren images showing the presence of shock waves at the nozzle exit have previously confirmed the supersonic gas speed in this configuration.[30,31] Figure 1a shows a scanning electron microscopy (SEM) image of the commercially available TiO_2 powder (98.6%, Yee-Yong Cerachem. Ltd., Korea), consisting of a mixture of 60% anatase and 40% rutile phases by

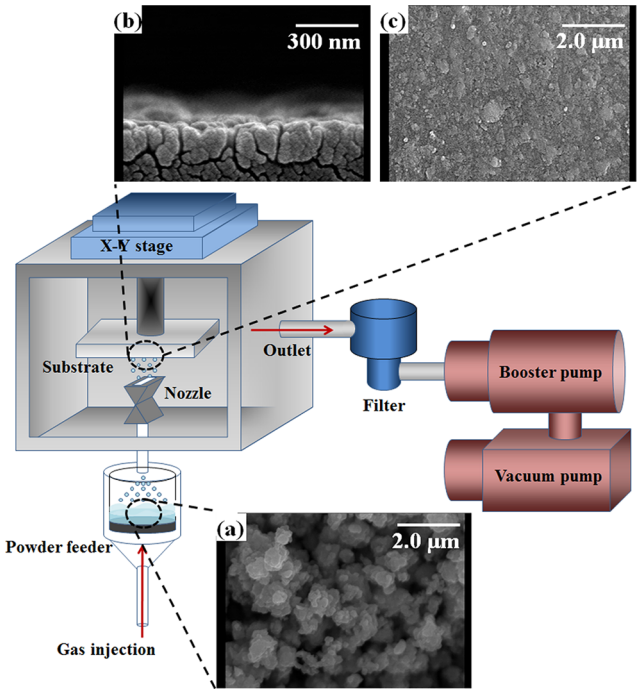

Figure 1. Schematic of the AD system. Insets include SEM images of (a) powder from which films were deposited and (b) side and (c) top views of as-deposited films.

Table 1. Typical Deposition Conditions

pressure in the deposition chamber [Torr]	0.35–5.6
propellant gas	air
nozzle exit area [mm^2]	10 × 35
stand-off distance [mm]	5
gas temperature	room temperature (20 °C)
consumption of the propellant gas [l/min]	10
stage traverse speed [mm/s]	0.72
no. of passes	1–2

weight. Agglomeration of the particles is clearly observed. To break up particle clusters, the powder was mixed with water, placed in a rotary evaporator, calcined at 400 °C, and then ball-milled for 24 h. This break-up process resulted in particles with an average size of approximately 0.5 μm. Such pretreated powders have been shown to have improved deposition rates compared to untreated powders.[32] Parts b and c of Figure 1 show the side and top views of the TiO_2 deposited film, respectively. The highly accelerated TiO_2 particles with irregular shapes collide at supersonic speed with the substrate, and their fragments are deposited.

The mass flow rate of the supply air was set to 10 L/min. For the average particle size of d_{50} = 0.5 μm, the Stokes number is St_k < 0.2, which implies that the particles attain in excess of 90% of the gas flow speed.[31] The Stokes number, $St_k = \tau_p/\tau_g$, is the ratio of the characteristic time for particles to respond to the surrounding flow, $\tau_p = \rho_p d^2/18\mu_g$, to the characteristic time of the surrounding flow, $\tau_g = D/u_{g,exit}$, where ρ_p and d are the particle density and diameter, μ_g is the gas dynamic viscosity, and D and $u_{g,exit}$ are the nozzle exit diameter and gas speed, respectively. The substrate was situated 5 mm away from the nozzle, which was installed onto a maneuvering stage that could move at speeds of up to 0.72 mm/s. For comparison, we prepared all TiO_2 films with equal thicknesses of about 150 nm. Although a uniform distribution of powder was desired across the nozzle exit, the particle number density at the nozzle center was likely to be greater than that at the periphery. The primary parameters influencing the coating quality were (1) the nozzle geometry, (2) the particle size and mass flow rate, (3) the air mass flow rate, and (4) the substrate stand-

off distance. All TiO_2 films were manufactured at room temperature on soda-lime glass substrates with a surface area of 1.0 × 3.5 cm^2 and roughness of R_a < 5 nm. Substrates were cleaned in acetone in an ultrasonic bath for 10 min before use.

The prepared TiO_2 films were characterized using several analytical techniques. A goniometer was used to record and measure the static water contact angle on as-deposited and annealed TiO_2 films. The contact angle was measured 1−2 h after annealing. The values were measured 5 s after the water drop touched the film surface. Deionized water was supplied to a stainless-steel nozzle (EFD; inner and outer diameters of 100 and 240 μm, respectively) by a syringe pump (KDS Legato 100) at a flow rate of 0.4 mL/min. All measurements and experiments were performed at ambient conditions and room temperature. The average static water contact angle value was obtained from measurements from at least five fresh positions on the same sample.

The microstructures and crystallinity of the deposited TiO_2 films were characterized by high-resolution SEM (XL30SFEG Phillips Co., Holland, at 10 kV) and X-ray diffraction (XRD; Rigaku Japan, D/MAX-2500), using Cu Kα radiation over a 2θ range of 20−50°. The surface topography and surface roughness were characterized by atomic force microscopy (AFM; Park Systems XE-100) in tapping mode. Fourier transform infrared (FT-IR) spectra were recorded on samples scraped from the substrate, mixed with KBr, pressed into a pellet, and measured in transmission mode in a Fourier-transform infrared spectrometer (Spectrum GX, Perkin-Elmer). The secondary-ion mass spectrometry (SIMS) measurements were carried out in a time-of-flight mass spectrometer (ION-TOF, Germany), which was equipped with a pulsed Ga^+ liquid ion gun operated at 15 kV. The ion-beam direct current (25 nA) was pulsed at a 5 kHz repetition rate, with a measured pulse width of about 8 ns. The analyzed area was approximately 300 × 300 μm^2. The total ion dose used to acquire each spectrum was about 9^{16} ions/cm^2, which ensures static SIMS conditions.

3. RESULTS AND DISCUSSION

3.1. Superhydrophilicity. The static water contact angle curve for the films annealed at different temperatures (27 < T_{anneal} < 550 °C) is shown in Figure 2. Higher annealing

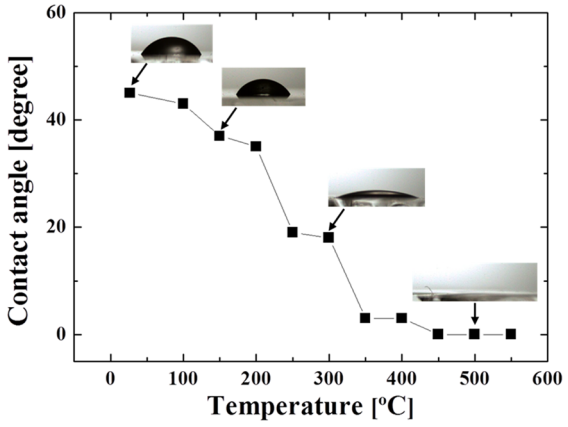

Figure 2. Relationship between the water contact angle and annealing temperature, without exposure to UV light.

temperatures (>550 °C) can lead to melting of the soda-lime glass substrate and thus were not used. The hydrophilic-to-superhydrophilic transition of the TiO_2 films occurred over a broad temperature range and was complete at around 450 °C. The films annealed at 500 °C showed the lowest water contact angle, exhibiting complete wetting ($\theta \sim 0°$); this hydrophilicity is a permanent phenomenon for which the measured contact angle (below 3°) was retained even after 3 months (Figure S1 in the Supporting Information). The as-deposited films exhibited modest hydrophilicity with a water contact angle of ∼45°. As the annealing temperature increased in the range of 100−300 °C, the water contact angle decreased remarkably from ∼43° to ∼19°. In the temperature range of 350−400 °C, the films became superhydrophilic, with a water contact angle of ∼5°. Above 450 °C, the films showed strong super-hydrophilic behavior, with a water contact angle of ∼0°. The water droplet spreads completely and instantaneously on the film annealed at 500 °C.

In Figure 3, XPS results at various temperatures are shown. The O 1s spectra revealed two different peaks for the TiO_2 film

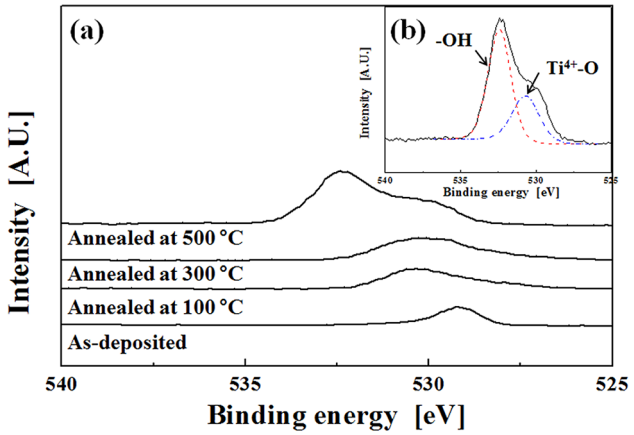

Figure 3. O 1s XPS spectrum of TiO_2 films (a) at various temperatures and (b) annealed at 500 °C (in the range of 525−540 eV).

annealed at 500 °C; the right peak is located at 529−530 eV, and the left peak is located at 530−532 eV (see the magnified image in Figure 3b). The first peak corresponds to the typical TiO_2 group, while the second peak corresponds to the −OH group. After annealing at 500 °C, a shoulder band (OH group on the left) appeared at 532.4 eV, which was not present in the as-deposited and TiO_2 films annealed at lower temperatures (100 and 300 °C). The shoulder peak indicated the presence of surface −OH groups, whose presence promotes super-hydrophilicity. For this reason, the greater the annealing temperature, the lower the water contact angle.

The wetting properties of TiO_2 films can depend on many factors, such as the composition, crystalline structure, surface roughness, and density of surface hydroxyls on the film surface. As shown so far, the annealing temperature strongly influenced the wetting properties of the TiO_2 surface. Increasing the annealing temperature decreased the water contact angle of the films, reflecting their increased hydrophilicity. Heating the surface to sufficiently high temperature can induce desorption of the surface oxygen, producing oxygen vacancies. One missing O atom at the bridging-O site leaves two subsurface Ti^{3+} sites exposed. Water molecules can react with these oxygen vacancies to produce surface OH groups, which tend to make the surface hydrophilic.[5] High-temperature annealing can also degrade organic contaminants that are responsible for hydrophobicity.[33] Several explanations for thermally induced hydrophilicity have been proposed, including the cleansing effect,[26] the crystal-phase transition,[28] the surface micro/nanostructure,[34] the effect of Ti^{3+} defect sites and oxygen vacancy sites,[35] and changes in surface roughness.[36]

3.2. Crystallinity and the Crystal Phase. As previously reported,[37] the temperature plays a fundamental role in determining the crystal structure of TiO_2 films. Figure 4

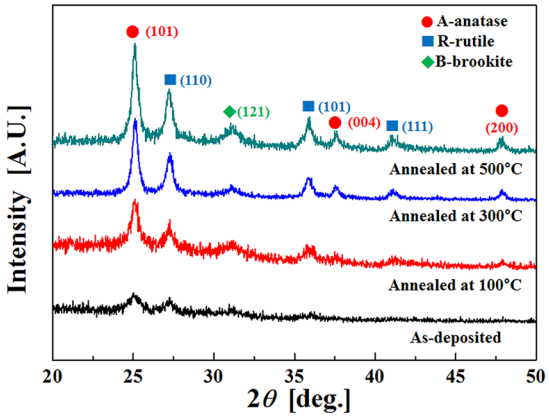

Figure 4. XRD patterns from the as-deposited film and films annealed at various temperatures.

shows the XRD patterns of as-deposited and annealed TiO_2 thin films (also available is Figure S2 in the Supporting Information showing the XRD pattern of the raw powder). The crystal structure of the films changes with increasing annealing temperature. The raw TiO_2 powder consists of 60% anatase and 40% rutile phases by weight. Figure 4 shows that all films are polycrystalline and possess peaks characteristic of the anatase, rutile, and brookite phases. The diffraction pattern of the as-deposited film shows peaks of minimal intensity, reflecting the fragmentation and decrease in crystallinity induced by the supersonic AD. The peak intensity increases as the film undergoes annealing. The peaks near 25.3°, 37.5°, and 48.1° can be assigned to the (101), (004), and (200) planes of the anatase phase (JCPDS 21-1272), while the peaks near 27.1°, 36.2°, and 41.1° are in good agreement with the (110), (100), and (111) planes of the rutile phase (JCPDS 21-1276). With increasing annealing temperature, a peak near 31.7° appears, which is assigned to the (121) plane of the brookite phase (JCPDS 29-1360).

Rietveld refinement was used to fit the diffraction patterns to a mixture of anatase, rutile, and brookite phases, as shown in the Supporting Information (Figure S3 and Table S1). As expected, the raw powder did not contain any brookite phase. For the as-deposited film and the film annealed at 100 °C, the fitting gives about 50% brookite in the films, but the fitted lattice parameters deviate significantly from the standard lattice parameters for brookite. The XRD peaks in these samples are broad and noisy because of the small crystallite size and likely presence of strain. Therefore, the fitted lattice parameters, phase fractions, and crystallite sizes are not expected to be quantitatively reliable. Nonetheless, these patterns clearly show that the supersonic AD process has resulted in a dramatic decrease in the crystallite size and crystallinity, along with the conversion of some of the more thermodynamically stable rutile and anatase phases into the metastable brookite phase. The XRD patterns from the films annealed at 300 and 500 °C are less noisy and can be reliably fit to a mixture of the three phases. These fits show that a substantial amount of brookite (~30%) is present in these films, along with rutile and anatase phases, and that the brookite lattice is somewhat distorted, with lattice parameters that differ slightly from the expected bulk values.

3.3. Surface Morphology and Surface Roughness. The surface morphology and surface roughness of TiO_2 films annealed at various temperatures were studied. Figure 5 shows

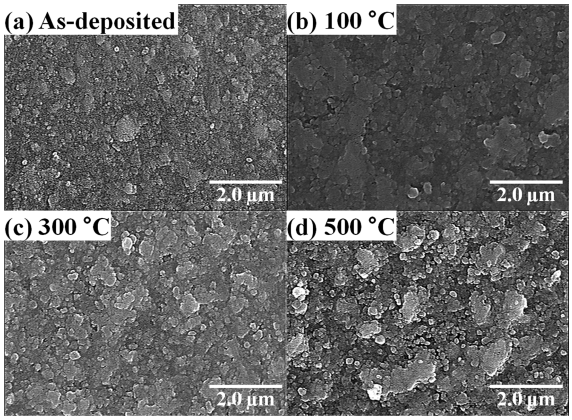

Figure 5. Top-view SEM micrographs of TiO_2 films on soda-lime glass: (a) as-deposited and annealed at (b) 100, (c) 300, and (d) 500 °C.

top-view SEM micrographs of (a) an as-deposited TiO_2 film and TiO_2 films annealed at (b) 100, (c) 300, and (d) 500 °C. The SEM images confirm the uniform and homogeneous deposition of TiO_2 nanoparticles over the soda-lime glass. The films were free of cracks and large aggregates, which accounts for the high mechanical stability of the films. The relatively smooth and nonporous morphology of the as-deposited TiO_2 film changes gradually to a more porous and granular morphology with increasing annealing temperature. Annealing appears to increase the cohesion between the TiO_2 particles as well as their adhesion to the substrate.

To explain the interrelations among their superhydrophilic behavior and surface roughness, AFM analyses were performed for the TiO_2 films annealed at different temperatures. The change in the surface roughness of the TiO_2 film with increasing annealing temperature can be seen in the 3D AFM images (Figure 6). The surface roughness (R_a) represents the root-mean-square average of the height difference between the surface points and the mean plane obtained by fitting the image data points. Compared with the as-deposited TiO_2 film, the TiO_2 film annealed at 500 °C exhibited a rougher surface with a

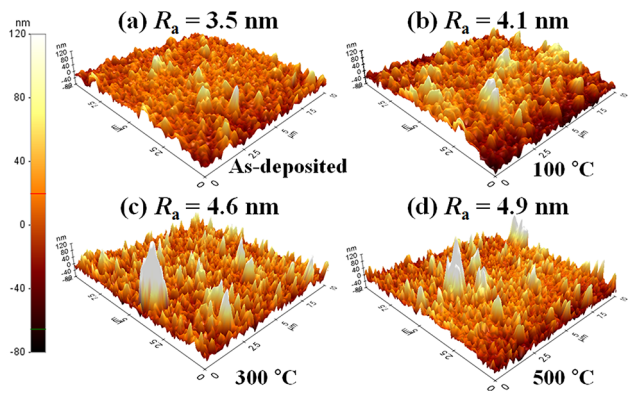

Figure 6. AFM images of TiO_2 films on a soda-lime glass: (a) as-deposited and annealed at (b) 100, (c) 300, and (d) 500 °C.

dx.doi.org/10.1021/am401083y | ACS Appl. Mater. Interfaces 2013, 5, 6155−6160

root-mean-square roughness of 4.9 nm, compared to a value of 3.5 nm for the as-deposited films. With increasing annealing temperature, conversion from the hydrophilic state to the superhydrophilic state was expedited. Interestingly, the surface roughness also increased with the annealing temperature, which, in turn, provided a larger interfacial area.[38] In addition, it is noteworthy that the TiO_2 film annealed at 500 °C was characterized by a high surface −OH content, as is evident by the XPS data (Figure 3).

3.4. Surface Hydroxyl Groups. Hydroxyl (−OH) groups present on the surface of TiO_2 films favor both the van der Waals forces and the hydrogen-bonding interactions between water and the surface. Thus, the hydrophilicity of the surface is expected to increase with increasing density of the surface hydroxyl groups.[39] The surface hydroxyls promote hydrophilicity, but the surface hydroxyls are not the only factor governing the surface properties. The FT-IR spectra of Figure 7

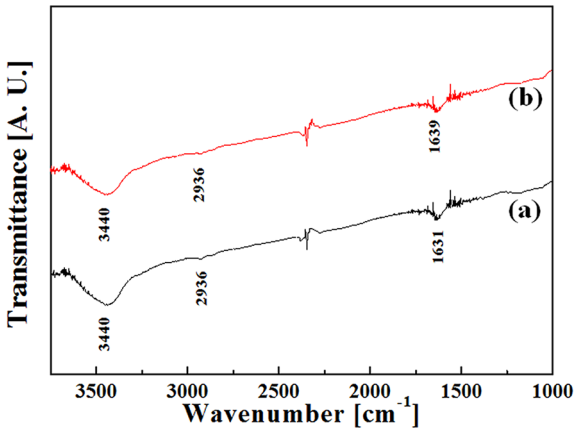

Figure 7. FT-IR spectra of TiO_2 films (a) as-deposited and (b) annealed at 500 °C.

show the clear presence of hydroxyl peaks at 1630 and 3440 cm^{-1} in the films. However, the apparent intensity of the hydroxyl peaks remained almost the same before and after annealing (at up to 500 °C). Without other significant IR peaks for comparison, we cannot firmly conclude that the hydroxyl coverage did not change. However, no change is obvious, and the hydroxyl coverage does not appear to be a key factor in determining the thermally induced hydrophilicity of these TiO_2 films.

Time-of-flight SIMS (TOF-SIMS) measurement was used to analyze the interfacial and chemical composition of the TiO_2 thin films, as shown in Figure 8. The TOF-SIMS depth profile confirms that there is no significant change in the hydroxyl group intensity with increasing substrate temperature from 100 to 500 °C. The SiO_2 peak normally comes from the silica glass substrate used for the deposition process. The presence of Si and SiO_2 fragments within the TiO_2 film suggests that an interfacial layer has formed by reactions among Ti, Si, and O atoms.

The thermally induced superhydrophilicity observed in our annealed films appears to arise from a combination of changes in the degree of crystallinity and the crystal polymorphs present in the film along with changes in the surface topography. The role of the crystalline phase on the hydrophilicity of the three TiO_2 polymorphs has been recently inferred by attenuated-total-reflectance FT-IR measurements on anatase, brookite, and rutile samples prepared without calcination treatments, with

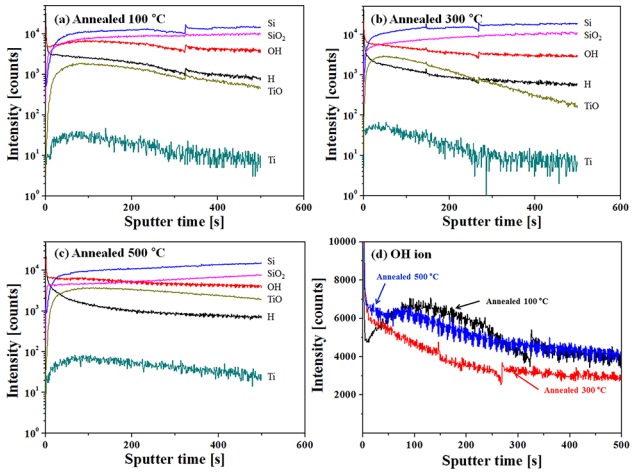

Figure 8. TOF-SIMS depth profile for the TiO_2 films annealed at (a) 100, (b) 300, (c) and 500 °C and (d) OH ions in the TiO_2 films annealed at 100, 300, and 500 °C.

brookite exhibiting the highest hydrophilicity, followed by anatase and then rutile.[40] Shibata et al.[41] also suggested that the brookite phase TiO_2 is more hydrophilic than the other polymorphs. In our case, at an annealing temperature of 500 °C, the crystallinity of the brookite phase was dramatically increased, which partially explains the observed superhydrophilicity. The increase in the crystallinity of the anatase and rutile phases at 500 °C can also contribute to the increase in hydrophilicity.[35] A porous microstructure[21] and increased surface roughness[6] have also been reported to increase hydrophilicity. In this work, the observed surface roughness of the TiO_2 films increases with increasing annealing temperature.

4. CONCLUSION

We have prepared nanostructured TiO_2 thin films by supersonic AD. The crystal structure, surface morphology, surface roughness, and superhydrophilicity depended strongly on the temperature at which the films were annealed after deposition. We produced superhydrophilic TiO_2 films without UV-light irradiation. The TiO_2 film annealed at 500 °C exhibited the best thermally induced superhydrophilicity. Moreover, the crystal structure, surface morphology, and surface roughness were shown to be the key factors that induce changes in film wettability. Most notably, the supersonic AD of the anatase and rutile precursor powder leads to substantial amorphization and fragmentation. Upon annealing, a substantial fraction of TiO_2 crystallizes as the metastable brookite phase, which is more hydrophilic than the anatase or rutile phase. Thus, supersonic AD followed by annealing provides a route to a nanostructured mixture of all three TiO_2 phases that exhibits superhydrophilicity without UV exposure. These results can benefit the design and manufacture of antifogging and self-cleaning superhydrophilic TiO_2 films.

■ ASSOCIATED CONTENT

Supporting Information

Additional water contact angles, XRD patterns, and Rietveld refinement fitting. This material is available free of charge via the Internet at http://pubs.acs.org.

AUTHOR INFORMATION

Corresponding Author

*E-mail: skyoon@korea.ac.kr.

Notes

The authors declare no competing financial interest.

ACKNOWLEDGMENTS

This work was supported by the Human Resources Development of the Korea Institute of Energy Technology Evaluation and Planning (KETEP; Grant 20124030200120) and the Converging Research Center Program through the Ministry of Education, Science and Technology (Grant 2010K000969).

REFERENCES

(1) Dunnill, C. W.; Parkin, I. P. *Dalton Trans.* **2010**, *40*, 1635−1640.
(2) Watanabe, T.; Nakajima, A.; Wang, R.; Minabe, M.; Koizumi, S.; Fujishima, A.; Hashimoto, K. *Thin Solid Films* **1999**, *351*, 260−263.
(3) Fujishima, A.; Rao, T. N.; Tryk, D. A. *J. Photochem. Photobiol., C* **2000**, *1*, 1−21.
(4) Parkin, I. P.; Palgrave, R. G. *J. Mater. Chem.* **2004**, *15*, 1689−1695.
(5) Wang, R.; Sakai, N.; Fujishima, A.; Watanabe, T.; Hashimoto, K. *J. Phys. Chem. B* **1999**, *103*, 2188−2194.
(6) Yu, J.; Zhao, X.; Zhao, Q.; Wang, G. *Mater. Chem. Phys.* **2001**, *68*, 253−259.
(7) Miyauchi, M.; Tokudome, H. *J. Mater. Chem.* **2007**, *17*, 2095−2100.
(8) Etacheri, V.; Seery, M. K.; Hinder, S. J.; Pillai, S. C. *Adv. Funct. Mater.* **2011**, *21*, 3744−3752.
(9) O'Regan, B.; Grfitzeli, M. *Nature* **1991**, *353*, 24.
(10) Grinis, L.; Kotlyar, S.; Rühle, S.; Grinblat, J.; Zaban, A. *Adv. Funct. Mater.* **2010**, *20*, 282−288.
(11) Mills, A.; Lee, S. K.; Lepre, A.; Parkin, I. P.; O'Neill, S. A. *Photochem. Photobiol. Sci.* **2002**, *1*, 865−868.
(12) Honda, H.; Ishizaki, A.; Soma, R.; Hashimoto, K.; Fujishima, A. *J. Illum. Eng. Soc.* **1998**, *27*, 42−49.
(13) Cai, R.; Kubota, Y.; Shuin, T.; Sakai, H.; Hashimoto, K.; Fujishima, A. *Cancer Res.* **1992**, *52*, 2346−2348.
(14) Choi, W.; Termin, A.; Hoffmann, M. R. *J. Phys. Chem.* **1994**, *98*, 13669−13679.
(15) Diebold, U. *Surf. Sci. Rep.* **2003**, *48*, 53−229.
(16) Pang, C. L.; Lindsay, R.; Thornton, G. *Chem. Soc. Rev.* **2008**, *37*, 2328−2353.
(17) Thomas, A. G.; Syres, K. L. *Chem. Soc. Rev.* **2012**, *41*, 4207−4217.
(18) Wenzel, R. N. *Ind. Eng. Chem* **1936**, *28*, 988−994.
(19) Damodar, R. A.; You, S. J.; Chou, H. H. *J. Hazard. Mater.* **2009**, *172*, 1321−1328.
(20) Liu, H.; Feng, L.; Zhai, J.; Jiang, L.; Zhu, D. *Langmuir* **2004**, *20*, 5659−5661.
(21) Huang, W.; Lei, M.; Huang, H.; Chen, J.; Chen, H. *Surf. Coat. Technol.* **2010**, *204*, 3954−3961.
(22) Hao, Y. Q.; Wang, Y. F.; Weng, Y. X. *J. Phys. Chem. C* **2008**, *112*, 8995−9000.
(23) Houmard, M.; Riassetto, D.; Roussel, F.; Bourgeois, A.; Berthomé, G.; Joud, J.; Langlet, M. *Surf. Sci.* **2008**, *602*, 3364−3374.
(24) Peng, B.; Tan, L.; Chen, D.; Meng, X.; Tang, F. *ACS Appl. Mater. Interfaces* **2011**, *4*, 96−101.
(25) Du, Y.; Gan, Y.; Yang, P.; Zhao, F.; Hua, N.; Jiang, L. *Thin Solid Films* **2005**, *491*, 133−136.
(26) Meng, F.; Xiao, L.; Sun, Z. *J. Alloys Compd.* **2009**, *485*, 848−852.
(27) Sebbowa, T.; Edirisinghe, M.; Salih, V.; Huang, J. *Biofabrication* **2011**, *3*, 045001.
(28) Lai, Y.; Tang, Y.; Gong, J.; Gong, D.; Chi, L.; Lin, C.; Chen, Z. *J. Mater. Chem.* **2012**, *22*, 7420−7426.
(29) Permpoon, S.; Houmard, M.; Riassetto, D.; Rapenne, L.; Berthomé, G.; Baroux, B.; Joud, J.; Langlet, M. *Thin Solid Films* **2008**, *516*, 957−966.
(30) Park, J. J.; Lee, M. W.; Yoon, S. S.; Kim, H. Y.; James, S. C.; Heister, S. D.; Chandra, S.; Yoon, W. H.; Park, D. S.; Ryu, J. *J. Therm. Spray Technol.* **2011**, *20*, 514−522.
(31) Lee, M.; Park, J.; Kim, D.; Yoon, S.; Kim, H.; Kim, D.; James, S.; Chandra, S.; Coyle, T.; Ryu, J. *J. Aerosol Sci.* **2011**, *42*, 771−780.
(32) Akedo, J. *J. Am. Ceram. Soc.* **2006**, *89*, 1834−1839.
(33) Ye, Q.; Liu, P.; Tang, Z.; Zhai, L. *Vacuum* **2007**, *81*, 627−631.
(34) Farbod, M.; Rezaian, S. *Thin Solid Films* **2011**, *520*, 1954−1958.
(35) Lu, G.; Linsebigler, A.; Yates, J. T., Jr. *J. Phys. Chem.* **1994**, *98*, 11733−11738.
(36) Wei, W.; Da-Wei, Z.; Chun-Xian, T.; Qi, W.; Wen-Na, W.; Yuan-Shen, H.; Zheng-Ji, N.; Song-Lin, Z.; Hai-Xia, L.; Ting, M. *Chin. Phys. Lett.* **2012**, *29*, 088103.
(37) Hou, Y. Q.; Zhuang, D. M.; Zhang, G.; Zhao, M.; Wu, M. S. *Appl. Surf. Sci.* **2003**, *218*, 98−106.
(38) Bekermann, D.; Gasparotto, A.; Barreca, D.; Devi, A.; Fischer, R. A.; Kete, M.; Lavrenčič Štangar, U.; Lebedev, O. I.; Maccato, C.; Tondello, E. *ChemPhysChem* **2010**, *11*, 2337−2340.
(39) Yu, J.; Zhao, X. *J. Mater. Sci. Lett.* **2001**, *20*, 671−673.
(40) Augugliaro, V.; Loddo, V.; López-Muñoz, M. J.; Márquez-Álvarez, C.; Palmisano, G.; Palmisano, L.; Yurdakal, S. *Photochem. Photobiol. Sci.* **2009**, *8*, 663−669.
(41) Shibata, T.; Irie, H.; Ohmori, M.; Nakajima, A.; Watanabe, T.; Hashimoto, K. *Phys. Chem. Chem. Phys.* **2004**, *6*, 1359−1362.